(4) P. Gans and S. M. E. Haque, *Chem. Ind. (London)*, 978 (1972).
(5) F. A. Cotton and D. L. Hunter, *Inorg. Chem.*, **13**, 2044 (1974).
(6) K. Honda, *Ann. Phys. (Leipzig)*, **32**, 1027 (1910).
(7) M. Owen, *Ann. Phys. (Leipzig)*, **37**, 657 (1912).
(8) R. S. Nicholson, *Anal. Chem.*, **37**, 1351 (1965).
(9) F. Hein and S. Herzog, *Z. Anorg. Chem.*, **267**, 337 (1952).
(10) M. Ciampolini and P. Paoletti, *Inorg. Chem.*, **6**, 1261 (1967).
(11) K. G. Caulton and R. F. Fenske, *Inorg. Chem.*, **7**, 1273 (1968).

Contribution from the Department of Chemistry,
Florida State University, Tallahassee, Florida 32306

Lattice Effects on the Electron Resonance of Halopentaamminechromium(III) Complexes

M. T. HOLBROOK and B. B. GARRETT*

Received June 19, 1975 AIC50434X

Powder electron resonance spectra have been used to study the effect of different counterions on the spin-Hamiltonian parameters of $[Cr(NH_3)_5Cl]^{2+}$ and $[Cr(NH_3)_5Br]^{2+}$ in the isomorphous hosts $[Co(NH_3)_5X]Y_2$ with Y^- = Cl^-, Br^-, I^-, and NO_3^-. X-ray powder patterns were used to determine the variations in the lattice dimensions. To explain the lattice effects a model with two different lattice deformations is necessary. The lattice effects are observed primarily through variations of the zero-field splitting tensor. Several possible lattice perturbation mechanisms are examined in the context of the origins of the zero-field splitting.

Introduction

Awareness of the effects of the lattice or environment on the electron paramagnetic resonance (EPR) spectra of molecular complexes of chromium(III) has been slow to develop. Most of the early studies of these systems were concerned with the contributions of the internal electronic structure to the spin-Hamiltonian parameters of the systems.[1,2] The large amount of effort involved in obtaining and interpreting single-crystal EPR data precluded comparison of the spectra in various host lattices. Thus, it was tacitly assumed that the paramagnetic complex adopted an intrinsic set of properties when it was substituted into an isomorphous host lattice. With the advent of random orientation spectra in glasses[3] and powders[4] it became feasible to begin comparison of the EPR spectra of a variety of related complexes.[3-10] The zero-field splittings of mixed-ligand complexes such as *trans*-$[Cr(en)_2A_2]^{n+}$,[3] $[Cr(NH_3)_5A]^{n+}$,[5,10] $[Cr(NH_3)_4AA']^{n+}$,[8,9] and $[Cr(py)_4AA']^{n+}$ [9] (en = ethylenediamine, py = pyridine) were found to vary systematically with the ligand field strength of the A ligand, but changes of up to 20% in the zero-field splittings were found for the same chromium complex in different host lattices or in the same lattice at different temperatures.[6-8] The relative magnitude of the lattice effects leaves intact the idea that the spin-Hamiltonian parameters are molecular properties, but at the same time, this sensitivity to the environment will be useful for the study of guest–host interactions and may yield information about the relative importance of the intramolecular origins of the spin Hamiltonian.

The retention of an essentially molecular spin Hamiltonian implies that the primary effect of the lattice is to perturb the intramolecular origins of this Hamiltonian. Thus, it is requisite that we review these origins. Attention is focused upon the zero-field splitting for convenience of discussion and because no significant lattice effects have been observed for the **g** tensor. The zero-field splitting is primarily a spin–orbit effect, being a remnant of the free-ion spin–orbit splitting. Formally, the crystal field quenches the coupling between spin and orbital angular momenta by destroying the spatial similarity of the d orbitals, but this quenching is incomplete because the spin–orbit interaction is strong enough to retain some rotational symmetry. This effect is described by an admixture of excited crystal field states back into the ground state. (For d^3 ions, the only nonvanishing spin–orbit matrix elements with the $^4A_2(O_h)$ ground state involve excited states of $^2T_2$ and $^4T_2(O_h)$ symmetry.) The axial zero-field parameter, D, reflects the difference between the spin–orbit effect about the z axis and about an axis in the xy plane while the rhombic parameter measures similar differences about the x and y directions.

The magnitude of the spin–orbit interaction is considerably altered by several molecular effects.[1,2] (a) Unpaired spin is transferred off the metal ion onto the ligands reducing the metal wave function coefficients in the molecular orbitals of both the ground state and the admixed excited states. This delocalization naturally reduces the spin–orbit matrix elements on the metal center. Stephens incorporated this effect into the crystal field descriptions by including an orbital reduction factor.[11] (b) Both the interelectron repulsion parameters observed in the optical spectra and the spin–orbit parameter, which depend upon $\langle r^{-1} \rangle$ and $\langle r^{-3} \rangle$, respectively, are reduced by radial expansion of the metal d orbitals.[12] The relationship between the optical nephelauxetic effect[13] and the spin–orbit parameter reduction has been quantified[14] so that the appropriate spin–orbit parameter for a complex ion may be estimated from the optical data. (c) Spin density which is delocalized onto the ligands is subjected to a potential characteristic of the ligand and thus suffers a spin–orbit interaction characteristic of the ligand center. This ligand spin–orbit effect opposes the spin–orbit interaction on the metal center in matrix elements connecting excited crystal field states to the ground state but augments the interaction on the metal in matrix elements involving (d) charge-transfer states. The contributions of the spin–orbit interaction on ligand centers and of the charge-transfer state admixture were first recognized and formulated by Lacroix and Emch.[15] Subsequent quantitative estimates indicate that the charge-transfer state matrix elements may account for as much as 40% of the axial zero-field splittings.[2,5] (e) Doublet-state admixture into the quartet ground state via the spin–orbit interaction has been considered by several authors[1,2,16] with discordant results, but this effect probably does not contribute more than 10% of the zero-field splitting of the chemically anisotropic systems under consideration in this paper. (f) The dipole–dipole interaction between the unpaired spins can also contribute to the zero-field

splitting but McGarvey[1] has estimated that contribution to be about 5% of the spin–orbit contribution using crystal field limit spin distributions. This estimate would be reduced by radial expansion and spin delocalization effects because the dipole–dipole interaction depends on $\langle r^{-3} \rangle$. Effects (a) through (d) contribute to the g tensor but (e) and (f) do not.

The zero-field splittings may also be discussed in terms of anisotropic spin–orbit interactions. Besides anisotropic electron distributions, this approach incorporates the concept that radial expansion effects may be different for orbitals belonging to different irreducible representations in the low-symmetry ligand field. This necessitates introduction of a separate spin–orbit parameter for each irreducible representation and still more parameters for spin–orbit matrix elements between different representations. Besides being hopelessly overparameterized, the effects of differential radial expansion and charge delocalization are inseparable in this model. The analogous separability problem in the optical nephelauxetic effect has been discussed in detail by Jorgensen.[17] Since the physical effects of the lattice can be discussed without loss of generality in terms of the orbital populations picture of the preceding paragraph, that model will be used henceforth.

The lattice may change the intermolecular spin Hamiltonian (a) through deformation of the geometry of the paramagnetic complex with consequent charge and spin redistribution, (b) through alteration of the excited-state energies which moderate the amount of spin–orbit admixture as energy denominators in the second-order perturbation expressions,[2,5] (c) through orbital quenching which can arise from direct contact interactions between the unpaired spin distribution of the paramagnetic guest and the charge density of the host molecules, and (d) through reduction of the symmetry which allows admixture of excited states which do not mix in the higher symmetry. The first of these lattice-coupling mechanisms is likely to be the most important because the zero-field splitting is primarily a reflection of the charge distribution via the spin–orbit effect.[1,2,5] Minor variations of the excited-state energies, which are all that the secondary crystal field (non nearest neighbor to the metal ion) can contribute, will have little effect on the spin–orbit mixing.[2] Orbital quenching by touching interactions in a lattice would correspond to an electrostatic nephelauxetic effect although a similar polarization quenching in alkali halide diatomics has been attributed to exchange interactions.[18] No theoretical formulation of such interactions has been attempted and the importance of these effects is not presently understood. Finally, the importance of the admixture of new states under lower symmetry may be dominant in systems of intrinsically high symmetry such as $[Cr(NH_3)_6]^{3+}$ where bending deformations are important,[7] but for systems with intrinsic bonding asymmetry, such as pentaammine and tetraammine complexes of chromium(III), these lower symmetry lattice effects will be of lesser importance. Thus, it appears that the lattice effects should be explicable in terms of deformation with some resort to simple ligand field comparisons.

Because of the similarities of interpretation of the random orientation EPR spectra for microcrystalline powders and glasses, it is necessary to emphasize that the techniques are not equivalent. In each case the paramagnetic guest ion is surrounded by and interacts with its host. Hempel and coworkers[3] correctly pointed out the existence of a lattice or "secondary field" contribution to the spin-Hamiltonian parameters in crystalline materials. They also suggested that the randomly oriented counterions and solvent molecules in glasses would contribute only to the width of the EPR lines, allowing one to associate the average parameters obtained from this broad-line spectrum with the "intrinsic" properties of the complex. However these "intrinsic" properties include environmental contributions, because the solvent and counterion arrangements in the vicinity of these highly charged molecules are not necessarily very random and because the strong solvation necessary to dissolve the paramagnetic complex generates a "secondary field" characteristic of the glass. The differences among glasses are obscured by the uncertainties of the parameters obtained from them which are about as large as the range of values observed in various crystalline hosts. These uncertainties in glasses are about 10 G ($\sim$0.001 cm^{-1}) in most favorable cases and more typically about 100 G. Crystalline powders on the other hand yield parameters accurate to within 1 or 2 G with occasional broad-line or overlapping line spectra giving about 5-G uncertainties.

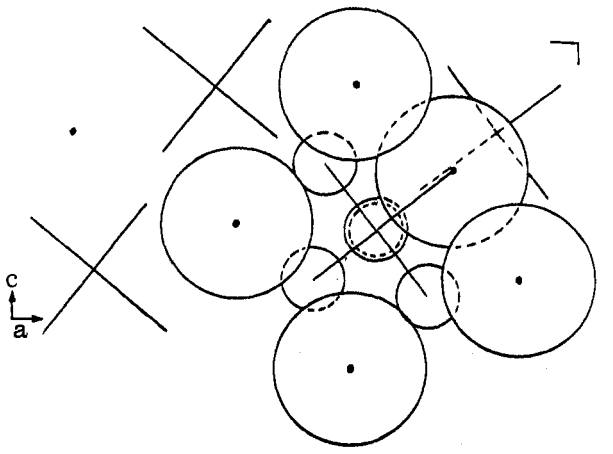

Figure 1. An *a–c* projection of $[Co(NH_3)_5Cl]Cl_2$ with one molecular ion and its nearest-neighbor counterions shown as spheres of the appropriate van der Waals radius.

The first powder EPR study of the halopentaamminechromium(III) complexes[5] failed to reveal any counterion or lattice dependence of the spectra even though a search for such effects was made. Real lattice effects became more apparent for systems of this type with the observation that the axial parameter, D, changed from 490 to 1160 G for $[Cr(NH_3)_6]^{3+}$ in $Co(NH_3)_6MCl_6$ for M = In and Bi, respectively.[7] Studies of the *trans*-diacidotetraamminechromium(III) complexes required the use of several host lattices for clarification of the mixed spectra and revealed lattice effects of up to 20% in the zero-field splittings.[8] Finally, increases in the value of D of about 15% with iron(III) complexes[5,6] and 7% for some chromium complexes, on lowering the temperature from 300 to 80 K, strongly suggested that there were significant lattice contributions to the zero-field splitting tensor. Pedersen and coworkers[9,10] have made similar observations for several tetragonal complexes of chromium(III).

In the present study, we consider the effect of counterion size on the zero-field splitting tensors for $[Cr(NH_3)_5X]^{2+}$ in a series of isomorphous host lattices of the formula $[Co(NH_3)_5X]Y_2$ with X^- = Cl^- or Br^- and Y^- = Cl^-, Br^-, I^-, or NO_3^-.[19] The orthorhombic crystals have *Pnma* (D_{2h}^{16}, No. 62) structure with a body-centered cubic arrangement of ions.[20] The large coordinated halogen of the body-centered cation extends through the face of the anion cube, severely distorting that cube. An *a–c* projection of the $[Co(NH_3)_5Cl]Cl_2$ unit cell is shown in Figure 1, where its nearest neighbors are shown as full circles of the appropriate van der Waals radius. A more detailed representation of the cation, $[Co(NH_3)_5Cl]^{2+}$, is shown in Figure 2, where the orientation and magnitudes of the root-mean-square displacements of the atoms are also illustrated.[20] We have measured the EPR spectra and unit cell dimensions for four host lattices for each of the chromium complexes considered. Changes in the EPR spectra with temperature and variation of the host cation will be presented later.

Table I. Spin-Hamiltonian Parameters for $[Cr(NH_3)_5X]Y_2$ in $[Co(NH_3)_5X]Y_2$ Host Lattices[a]

	D, G	E, G	g_z	g_y	g_x
$[Cr(NH_3)_5Cl]Cl_2$	950.1	47.3	1.9853	1.9858	1.9861
$[Cr(NH_3)_5Cl]Br_2$	852 (3)[a]	6 (6)	1.9843 (6)	1.9856 (3)	1.9855 (3)
$[Cr(NH_3)_5Cl]I_2$	702	85	1.9837	1.9857	1.9860
$[Cr(NH_3)_5Cl](NO_3)_2$	767	4	1.9848 (5)	1.9861 (3)	1.9863 (4)
$[Cr(NH_3)_5Br]Cl_2$	2276 (5)	37 (3)	1.9898 (4)	1.9916 (8)	1.9933 (5)
$[Cr(NH_3)_5Br]Br_2$	2224	23 (7)	1.9871 (4)	1.9921 (8)	1.9922 (4)
$[Cr(NH_3)_5Br]I_2$	2182 (5)	111 (4)	1.9847 (13)	1.9928 (4)	1.9930
$[Cr(NH_3)_5Br](NO_3)_2$	2127	8 (5)	1.9848 (4)	1.9921	1.9920

[a] The uncertainties are ≤2 in the last digit unless a larger uncertainty is given in parentheses.

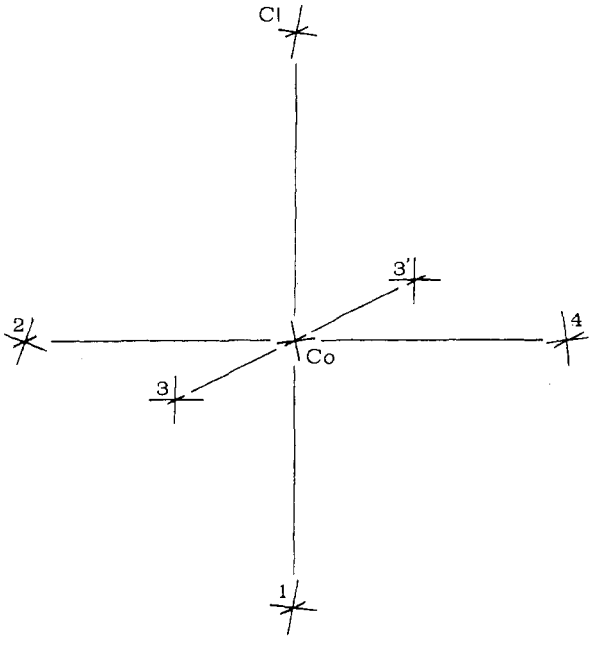

Figure 2. Orientations of the thermal ellipsoids within the complex ion of $[Co(NH_3)_5Cl]Cl_2$ (see Appendix).

Experimental Section

Starting materials $[Cr(NH_3)_5Cl]Cl_2$, $[Cr(NH_3)_5Br]Br_2$, $[Co(NH)_5Cl]Cl_2$, and $[Co(NH_3)_5Br]Br_2$ were all obtained by standard preparations involving heating the aquopentaammine complex in the presence of HCl or HBr.[21-23] These materials were separately ground with cold concentrated H_2SO_4 until HCl or HBr ceased to evolve. The very soluble sulfate or bisulfate salt of the complex was dissolved in water and reprecipitated with excess H_2SO_4. Mixed crystals were obtained by dissolving about 0.002 g of the chromium salt with about 0.1 g of the cobalt salt in 50 ml of water in an ice bath and adding a few drops of a concentrated solution of the desired counterion. When crystal growth began, a few more drops of counterion solution were added and crystal growth was allowed to continue. Samples were separated from solution before noticeable decomposition began (1 hr with bromo complexes and 3–4 hr with chloro complexes). The crystals were filtered, washed with ethanol and acetone, and allowed to air-dry before grinding into a very fine powder for x-ray and EPR measurements.

Electron resonance spectra were taken on a Varian E12 spectrometer at 35 GHz. Line positions were measured with a Spectromagnetic Industries NMR gaussmeter, Model 5200, and were reproducible to within ±1 G or better depending on the line shape. Diphenylpicrylhydrazyl (DPPH, $g = 2.0038$) was used as an internal standard to calibrate the microwave frequency. Spectra were fitted by exact diagonalization of the d^3 spin Hamiltonian. For each case, two or more samples were separately synthesized from the beginning to avoid the possibility of cross contamination of counterions. The spin-Hamiltonian parameters were reproducible and are presented in Table I.

Powder x-ray diffraction patterns were obtained with a Debye–Scherrer camera using copper radiation with a nickel filter for each of the host lattices in this study. The diffraction lines were assigned with the aid of the structure factors given in the single-crystal structure determinations.[19,20] Unit cell dimensions were obtained with a multiparameter least-squares analysis developed for the purpose. Fifteen to twenty-five diffraction lines were fitted to within a few parts per thousand with a consistent line assignment for the various lattices. Only 15 lines were obtainable for the nitrates because several lines expected to derive considerable intensity from the counterion scattering[19] were absent for these samples. The unit cell dimensions for the different host lattices are given in Table II. Densities calculated from these data agree with the experimentally determined densities of the halide salts.[24] Reliable density data were unavailable for the nitrate salts.

Table II. Unit Cell Dimensions (A) of $[Co(NH_3)_5X]Y_2$ with Orthorhombic *Pnma* (D_{2h}^{16}) Structure

Compd	a	b	c
$[Co(NH_3)_5Cl]Cl_2$	13.26	10.34	6.72
$[Co(NH_3)_5Cl]Br_2$	13.61	10.51	7.00
$[Co(NH_3)_5Cl]I_2$	14.34	10.69	7.51
$[Co(NH_3)_5Cl](NO_3)_2$	14.66	11.20	7.79
$[Co(NH_3)_5Br]Cl_2$	13.32	10.44	6.71
$[Co(NH_3)_5Br]Br_2$	13.50	10.63	7.02
$[Co(NH_3)_5Br]I_2$	14.28	10.85	7.41
$[Co(NH_3)_5Br](NO_3)_2$	14.65	11.49	7.71

Discussion

The unit cell dimensions of the various host lattices given in Table II increase in a nearly linear manner with respect to the radii of the halide anions which are taken to be 1.8 Å for chloride, 1.96 Å for bromide, 2.2 Å for iodide; nitrate is an oblate spheroid with a 2.6-Å major axis and a 1.4-Å minor axis. Extrapolation of the halide curves to the larger nitrate radius gives reasonable agreement for the b dimension, but the a and c dimensions fall below the extrapolation. The large dimension of the nitrate ion was used for these correlations because preliminary temperature-dependent EPR data suggest that the nitrate ion is tumbling at room temperature. The principal value of the x-ray powder studies is to verify that the structures, including the nitrates, are isomorphous; thus it is possible to discuss the lattice effects in terms of the same mechanisms for these hosts.

This study has demonstrated that the zero-field splitting of halopentaamminechromium(III) complexes is lattice dependent in a series of isomorphous host lattices. A comparison of the data in Table I shows that the axial parameter, D, decreases systematically with increase in counterion size while the rhombic parameter, E, is more erratic. The **g** tensor is apparently not very dependent upon the lattice even though the g-shift deviation from the free-electron $g = 2.0023$ arises from the same spin–orbit matrix elements with excited quartet states which contribute to the zero-field splitting. The dependence on the spin–orbit interaction is linear for the g-shift and quadratic for the zero-field splitting. The z component of the **g** tensor appears to follow the variation in D for both chloro and bromo complexes, but the effect is very near the limit of reliability of the data. The x and y components of the **g** tensor show no lattice effect. If there is a real lattice effect on g_z, then it presumably arises in the same way as the variation in the zero-field splitting.

We next examine the rhombic parameter, E, in order to clarify the total tensor contributions reflected in this parameter

before embarking on a more detailed discussion of D. As mentioned previously, E is erratic in these lattices. There is at most a small rhombic term in the nitrate and bromide hosts while the chloride and iodide hosts impose larger rhombic perturbations. It is conceivable that the entirety of the lattice effect could arise from equatorial (xy-plane) perturbation of the paramagnetic complex, but this can be ruled out by the following considerations. A maximal axial contribution would arise from an equatorial perturbation localized along a single axis because of the angular dependence ($3\cos^2\theta - 1$) of such perturbations. Augmenting interactions along the x and y axes would tend to cancel each other in their axial contribution. Thus the maximal axial contribution of an equatorial perturbation is $-E/2$. The changes of D for $[Cr(NH_3)_5Cl]^{2+}$ in the various lattices are too large relative to E to be accounted for in this manner. The changes of D from one lattice to another for $[Cr(NH_3)_5Br]^{2+}$ might be accounted for by appropriate choice of the signs of the E values, but the overall range of D is too large to be explained by an equatorial mechanism alone. Thus it is necessary to invoke separate mechanisms to explain the variations of D and E. A similar case arose for the zero-field splitting of the ferric ion in the charge-inverted but isomorphous $(NH_4)_2[InCl_5H_2O]$ host for which there is a large temperature-independent rhombic parameter but a strongly temperature-dependent axial parameter.[6]

The origin of the rhombic zero-field splitting is not made obvious either by the lattice variations or by the detailed crystal structure data for $[Co(NH_3)_5Cl]Cl_2$. In this lattice the trans-equatorial nitrogens, N_2 and N_4, have slightly longer bond lengths than N_3 and N_3' and the thermal ellipsoid of N_2 is essentially isotropic while the remaining nitrogens and Cl_1 have strongly anisotropic thermal parameters (see Figure 2 and the Appendix). A further illustration of the rhombic symmetry at the cobalt site in $[Co(NH_3)_5Cl]Cl_2$ is the ^{59}Co quadrupole asymmetry parameter[25] $\eta = 0.25$ which compares with the analogous EPR parameter $3E/D = 0.15$ for the chromium guest complex in this lattice. These features certainly justify the magnitude of E in $[Co(NH_3)_5Cl]Cl_2$ but no generalization applicable to the other lattices is forthcoming. If the rhombic parameter arose from specific packing arrangements in this lattice, then changes in the lattice dimensions over a large temperature range would cause a significant temperature dependence of E, but preliminary studies indicate that E is independent of temperature over the range from 100 to 540 K. This appears to be in contradiction with the obvious lattice dependence of E. A more extensive knowledge of the detailed crystal structures of several hosts and more extensive temperature-dependent EPR studies are needed to clarify the origins of the rhombic parameters in these systems.

The axial zero-field splitting parameter, D, consists of a large intramolecular or intrinsic part arising from the bonding asymmetry of the ligands, an axial lattice contribution from deformations of the complex, and a smaller axial projection of the equatorial mechanism discussed above. For $[Cr(NH_3)_5Cl]^{2+}$, D ranges from 700 to 950 G in the lattices studied here although larger values have been recorded in other environments.[8] A smaller range of D values, 2125–2275 G, was observed for $[Cr(NH_3)_5Br]^{2+}$, but the trend to smaller D with larger counterions is preserved. The lattice contribution may be of either sign relative to the internal D for these chemically anisotropic systems, the important feature being that D will decrease in magnitude if the lattice contribution makes the set of ligands more nearly cubic with respect to the metal ion. This could be accomplished in the systems under study either by increasing the average ligand field strength along the X–Cr–N_1 axis or by reducing the equatorial ligand field strength. An obvious axial mechanism is illustrated in Figure 1 where the projection of the centers of the counterion spheres on the coordinated chlorine–metal bond can be seen to give a resultant outward force on the bound chlorine reducing the effective ligand field along this axis. This mechanism would be expected to yield a reduced value for D at higher temperatures as the lattice expands and this has been observed in preliminary studies. Larger counterions will be displaced further from the metal and will contribute less outward repulsion of the bound halide. This increases the ligand field due to the bound halide and thus reduces the axial zero-field splitting. The thermal ellipsoids for $[Co(NH_3)_5Cl]Cl_2$ described in the Appendix and illustrated in Figure 2 offer some support for this mechanism because the major displacement axis of the bound chlorine lies along the bond direction. The equatorial nitrogens (N_2, N_3, N_3', and N_4) have their short displacement axes along the bond direction as expected whereas the axial nitrogen, which also appears to have its displacements channeled by counterions, has its primary displacement along the bond. This axial mechanism would be of the same sign as the intrinsic D and would tend to suggest that the intramolecular contribution to D is somewhat smaller than the observed D values in these systems, but the results in glasses,[3,9,10] other hosts,[8] and the additivity relations observed in trans-disubstituted tetraamminechromium(III) complexes[8,9] suggest larger intramolecular terms.

Both the axial and equatorial lattice effects observed in this study appear to be associated with physical deformations of the guest complexes by the hosts. Effects arising from changes of the energy separation of excited states from the ground state and from the introduction of new excited state admixtures by symmetry lowering do not appear to be important in the lattice variations observed here. Neither does the direct contact orbital quenching effect appear to make a contribution. This latter mechanism would be most likely to occur for large polarizable counterions such as iodide but would be less important for counterions such as chloride and nitrate. The fact that nitrate counterions have a lattice effect similar to the iodide in accordance with size considerations would suggest that contact quenching is not significant in these systems. It may be possible to select other systems which would make such effects more obvious. The present study has only begun the

Table III. Root-Mean-Square Displacements and Orientation of the Thermal Ellipsoids for the Atoms in $[Co(NH_3)_5Cl]Cl_2$

Atom	Approx molecular axis[a]	$(\bar{r}^2)^{1/2}$	Direction cosines rel to cryst axes		
			a	b	c
Co	z	0.14$_7$	0.8741	0	0.4857
	x	0.14$_3$	0.4857	0	−0.8741
	y	0.12	0	1	0
Cl_1	z	0.20	0.6363	0	0.7175
	x	0.15	−0.7715	0	0.6363
	y	0.17	0	1	0
N_1	z	0.20	−0.6617	0	−0.7498
	x	0.17	0.7498	0	−0.6617
	y	0.17	0	1	0
N_2	z	0.17	−0.3955	0	−0.9185
	x	0.18	0.9185	0	−0.3955
	y	0.18	0	1	0
N_3	z	0.18	−0.7310	−0.0809	−0.6776
	x	0.21	0.6779	0.0279	−0.7346
	y	0.13	0.0783	−0.9963	0.0344
N_4	z	0.21	0.8342	0	0.5514
	x	0.16	0.5514	0	−0.8342
	y	0.19	0	1	0
Cl_2		0.19	0.8599	−0.4482	−0.2445
		0.18	0.3573	0.1862	0.9152
		0.15	−0.3646	−0.8743	0.3203

[a] The molecular axis system is defined as $z \equiv$ Co–Cl_1 bond, $y \equiv b$ (crystal axis near the Co–N_3 bond), and $x \equiv$ normal to xy plane (near the Co–N_2 bond).

examination of lattice effects with EPR powder techniques and a variety of further studies are needed. Studies of the temperature dependence of these lattice effects and of the effect of host lattice cation variations are in progress. We have attempted to define some of the possible origins of lattice contributions both to systemize and to stimulate further work.

Appendix

The transformation of the anisotropic temperature factors to root-mean-square displacements along the principal axes of the thermal ellipsoids, given by Messmer and Amma[20] is incorrect. Their Table 4 should be replaced by Table III which refers the thermal ellipsoids to the crystal coordinates *a*, *b*, and *c*. A molecular coordinate system with *z* along the Co–Cl_1 bond, with *y* along the crystalline *b* axis which is approximately parallel to the Co–N_3 bond, and with *x* normal to the *yz* plane coincides with all the thermal ellipsoids of the molecular ion within experimental error and the correlation is indicated in Table III. This information is also illustrated in Figure 2. The fact that the non-symmetry-constrained principal axes of the ellipsoids for Cl_1, N_1, N_3, and N_4 coincide with the molecular axes lends strong credence to these parameters as real properties of the system.

Registry No. $[Cr(NH_3)_5Cl]Cl_2$, 13820-89-8; $[Cr(NH_3)_5Cl]Br_2$, 57255-92-2; $[Cr(NH_3)_5Cl]I_2$, 57255-93-3; $[Cr(NH_3)_5Cl](NO_3)_2$, 57255-94-4; $[Cr(NH_3)_5Br]Cl_2$, 57255-95-5; $[Cr(NH_3)_5Br]Br_2$, 13601-60-0; $[Cr(NH_3)_5Br]I_2$, 57255-96-6; $[Cr(NH_3)_5Br](NO_3)_2$, 57255-97-7; $[Co(NH_3)_5Cl]Cl_2$, 13859-51-3; $[Co(NH_3)_5Cl]Br_2$, 13601-43-9; $[Co(NH_3)_5Cl]I_2$, 37922-32-0; $[Co(NH_3)_5Cl](NO_3)_2$, 13842-33-6; $[Co(NH_3)_5Br]Cl_2$, 13601-38-2; $[Co(NH_3)_5Br]Br_2$, 14283-12-6; $[Co(NH_3)_5Br]I_2$, 14591-70-9; $[Co(NH_3)_5Br](NO_3)_2$, 21333-43-7.

References and Notes

(1) B. R. McGarvey, *J. Chem. Phys.*, **41**, 3143 (1964).
(2) B. B. Garrett, K. DeArmond, and H. S. Gutowsky, *J. Chem. Phys.*, **44**, 3393 (1966).
(3) J. C. Hempel, L. O. Morgan, and W. B. Lewis, *Inorg. Chem.*, **9**, 2064 (1970).
(4) L. E. Mohrmann, Jr., B. B. Garrett, and W. B. Lewis, *J. Chem. Phys.*, **52**, 535 (1970).
(5) L. E. Mohrmann, Jr., and B. B. Garrett, *Inorg. Chem.*, **13**, 357 (1974).
(6) G. M. Cole, Jr., and B. B. Garrett, *Inorg. Chem.*, **13**, 2680 (1974).
(7) E. W. Stout, Jr., and B. B. Garrett, *Inorg. Chem.*, **12**, 2565 (1973).
(8) S. J. Baker and B. B. Garrett, *Inorg. Chem.*, **13**, 2683 (1974).
(9) E. Pedersen and H. Toftlund, *Inorg. Chem.*, **13**, 1603 (1974).
(10) E. Pedersen and S. Kallesoe, *Inorg. Chem.*, **14**, 85 (1975).
(11) K. W. H. Stephens, *Proc. R. Soc. London, Ser. A*, **219**, 542 (1953).
(12) W. Marshall and R. Stuart, *Phys. Rev.*, **123**, 2048 (1961).
(13) C. E. Schaffer and C. K. Jorgensen, *J. Inorg. Nucl. Chem.*, **8**, 143 (1958).
(14) G. M. Cole and B. B. Garrett, *Inorg. Chem.*, **9**, 1898 (1970).
(15) R. Lacroix and G. Emch, *Helv. Phys. Acta*, **35**, 592 (1962).
(16) L. L. Lohr, Jr., and W. N. Lipscomb, *J. Chem. Phys.*, **38**, 1607 (1963).
(17) C. K. Jorgensen, *Adv. Chem. Phys.*, **5**, 33 (1963).
(18) (a) H. W. De Wijn, *J. Chem. Phys.*, **44**, 810 (1966); (b) J. LaPlante and A. D. Bandrauk, *Can. J. Chem.*, **52**, 2143 (1974).
(19) C. D. West, *Z. Kristallogr., Kristallgeom., Kristallphys., Kristallchem.*, **91**, 181 (1935).
(20) G. G. Messmer and E. L. Amma, *Acta Crystallogr., Sect. B*, **24**, 412 (1968).
(21) M. Mori, *Inorg. Synth.*, **5**, 131 (1957).
(22) E. Zinato, R. Lindholm, and A. W. Adamson, *J. Inorg. Nucl. Chem.*, **31**, 446 (1969).
(23) G. Schlessinger, "Inorganic Laboratory Preparations", Chemical Publishing Co., New York, N.Y., 1962, p 210.
(24) R. Klement, *Z. Anorg. Allg. Chem.*, **160**, 165 (1927).
(25) I. Watanabe, H. Tanaka, and T. Shimizu, *J. Chem. Phys.*, **52**, 4031 (1970).

Contribution from the Department of Chemistry, University of New Mexico, Albuquerque, New Mexico 87131

Tartrate-Bridged Chromium(III) Complexes. Synthesis and Characterization[1]

G. L. ROBBINS and R. E. TAPSCOTT*

Received July 15, 1975 AIC504990

The syntheses and properties of the tartrate-bridged complexes $[Cr_2(tartH)_2L_2]$ and $Na[Cr_2(tart)(tartH)L_2]$ ("tart" = $C_4H_2O_6^{4-}$, "tartH" = $C_4H_3O_6^{3-}$, L = 1,10-phenanthroline or 2,2'-bipyridyl) having either two optically active or two meso bridging ligands are described. The results of formula weight determinations prove a binuclear structure. The *ms*-tartrate derivatives are the first *ms-ms* isomers to be reported for a tartrate-bridged complex and, as predicted from steric considerations, both octahedral coordinations in these *ms-ms* isomers have the same chirality (Δ or Λ). The *ms*-tartrato–bipyridyl complex has been resolved and a $\Lambda\Lambda$ absolute configuration assigned to the $(+)_{589}$ enantiomer. Complexes containing two bridging groups of the same enantiomeric configuration are formed in preference to a complex with bridges of opposite chirality. Strong intramolecular hydrogen bonding probably accounts for the low acidity of the tartrato(4–)–tartrato(3–) compounds.

Introduction

The binuclear structure exhibited by a number of tartrate complexes[2-6] has been of interest owing, in part, to the large

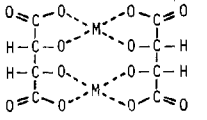

stereoselective effects observed in molecules having such a geometry[2,7,8] and to the exchange coupling found for some tartrate-bridged metal ion pairs.[9,10] Since varying combinations of tartrate isomers (*d* = *S,S*; *l* = *R,R*; meso = *R,S*) and, in some complexes, a dissymmetric coordination geometry may be present, an extensive isomerism is possible for tartrate-bridged complexes. The relative stabilities of the isomers have been explained in terms of the steric constraints of the binuclear structure and the conformations of the bridging tartrate groups and depend strongly on the coordination geometry.[2]

Of particular interest is the stereochemistry of binuclear tartrates containing octahedral metal ions since this geometry is sterically more favorable than tetragonal or trigonal bipyramidal coordinations, the coordination geometries of most of the previously studied tartrate-bridged structures,[3] for *ms*-tartrate bridging.[2,11] No binuclear metallotartrates containing meso bridges have heretofore been reported. Of the 24 isomers possible for tartrate-bridged octahedral complexes, the two enantiomeric pairs $\Delta\Delta(dd)$, $\Lambda\Lambda(ll)$ and β-$\Delta\Delta(ms\text{-}ms)$, β-$\Lambda\Lambda(ms\text{-}ms)$ (Figure 1)[12] are expected to be the energetically most stable.[2,11] The designation "β" distinguishes the more stable enantiomeric pair of bis(meso) isomers from the α pair which has the opposite orientation for

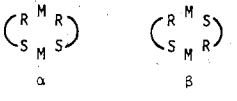

the rotationally nonequivalent chiral (*R* and *S*) extremities of the meso bridges. A related structural variation is possible for mononuclear octahedral chelates with meso bidentates.[13]

In an initiation of a study of the stereochemistry of octa-